# Origin of the spin reorientation transitions in $(Fe_{1-x}Co_x)_2B$ alloys

Kirill D. Belashchenko,[1] Liqin Ke,[2] Markus Däne,[3] Lorin X. Benedict,[3] Tej Nath Lamichhane,[2,4] Valentin Taufour,[2,4] Anton Jesche,[2,4] Sergey L. Bud'ko,[2,4] Paul C. Canfield,[2,4] and Vladimir P. Antropov[2]

[1)] *Department of Physics and Astronomy and Nebraska Center for Materials and Nanoscience, University of Nebraska-Lincoln, Lincoln, Nebraska 68588, USA*

[2)] *Ames Laboratory, U.S. Department of Energy, Ames, Iowa 50011, USA*

[3)] *Lawrence Livermore National Laboratory, Livermore, California 94550, USA*

[4)] *Department of Physics and Astronomy, Iowa State University, Ames, Iowa 50011, USA*

(Dated: 2 February 2015)

Low-temperature measurements of the magnetocrystalline anisotropy energy $K$ in $(Fe_{1-x}Co_x)_2B$ alloys are reported, and the origin of this anisotropy is elucidated using a first-principles electronic structure analysis. The calculated concentration dependence $K(x)$ with a maximum near $x = 0.3$ and a minimum near $x = 0.8$ is in excellent agreement with experiment. This dependence is traced down to spin-orbital selection rules and the filling of electronic bands with increasing electronic concentration. At the optimal Co concentration, $K$ depends strongly on the tetragonality and doubles under a modest 3% increase of the $c/a$ ratio, suggesting that the magnetocrystalline anisotropy can be further enhanced using epitaxial or chemical strain.

Magnetocrystalline anisotropy (MCA) of a magnetic material is one of its key properties for practical applications, large easy-axis anisotropy being favorable for permanent magnets.[1] Intelligent search for new materials requires understanding of the underlying mechanisms of MCA. This can be particularly fruitful for substitutional alloys whose properties can be tuned by varying the concentrations of their components. The analysis is often relatively simple in insulators, where MCA is dominated by single-ion terms which can be deduced from crystal-field splittings and spin-orbital (SO) selection rules. In contrast, in typical metallic alloys the band width sets the largest energy scale, and MCA depends on the details of the electronic structure.

The $(Fe_{1-x}Co_x)_2B$ solid solution[2–6] (space group $I4/mcm$[7]) is a remarkable case in point. $Fe_2B$ has a fairly strong easy-plane MCA, and $Co_2B$, at low temperatures, a small easy-axis MCA. However, the alloy has a substantial easy-axis MCA around $x = 0.3$,[2] making it a potentially useful rare-earth-free[8] permanent magnet. At $x \approx 0.5$ the MCA again turns easy-plane, peaks at $x = 0.8$, and then turns easy-axis close to $x = 1$. These three spin reorientation transitions must be related to the continuous evolution of the electronic structure with concentration. The goal of this Letter is to elucidate the origin of this rare phenomenon.

First, we report the results of experimental measurements at low temperatures. Single crystals of $(Fe_{1-x}Co_x)_2B$ were grown from solution growth out of an excess of (Fe,Co) which was decanted in a centrifuge.[9] The single crystals were grown as tetragonal rods which were cut using a wire saw to give them the shape of a rectangular prism. The demagnetization factor was calculated using Ref. 10. Field-dependent magnetization measurements were performed in a Quantum Design MPMS at 2 K in fields up to 5.5 T. The MCA energy $K$ was determined as the area between the two magnetization curves, with the field parallel and perpendicular to the $c$ axis, taken at the same temperature.[6] The results shown in Fig. 1 (blue stars) measured at 2 K confirm the non-monotonic concentration dependence, in good agreement with the measurements at 77 K from Ref. 2.

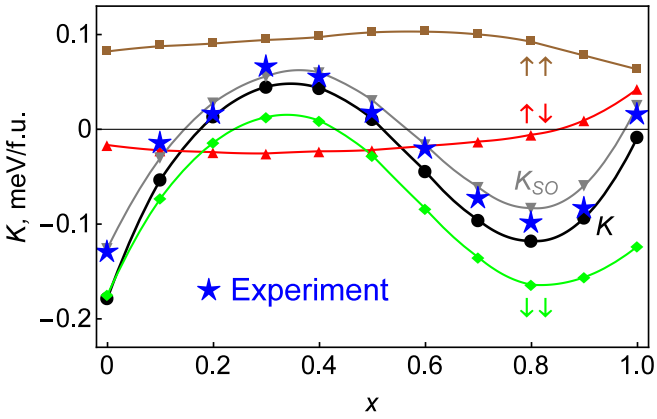


FIG. 1. Calculated (black circles) and experimental (blue stars) MCA energy $K$ in $(Fe_{1-x}Co_x)_2B$ alloys. Gray curve: $K_{SO}$. The other lines show the spin decomposition $K_{\sigma\sigma'}$.

Density-functional calculations using several different methods show that the choice of the exchange-correlation potential and other computational details strongly affect the calculated MCA in $Fe_2B$ and $Co_2B$. We have ascertained that this sensitivity is largely due to the variation of the exchange splitting, which controls the position of the Fermi level relative to the minority-spin bands. The systematic variation of MCA with $x$ is also controlled by the Fermi level shift. This continuous variation is, therefore, reliably predicted as long as the end points are correctly fixed using experimental input.

The results reported below were obtained using the Green's function-based formulation of the tight-binding linear muffin-tin orbital (GF-LMTO) method.[11] Substitutional disorder was treated using our implementation of the coherent potential approximation (CPA),[12] with the SO coupling included perturbatively as described in

the supplementary material.[13]

The lattice constants and the internal coordinates are linearly interpolated between the experimental data for the end compounds extrapolated to zero temperature:[2] $a = 5.109$ and 4.997 Å, $c = 4.249$ and 4.213 Å, and $u = 0.166$ and 0.168 for $Fe_2B$ and $Co_2B$, respectively. The exchange and correlation are treated within the generalized gradient approximation (GGA).[14]

The correct exchange splitting at the end points can be enforced by using the experimental data[2–6] for the magnetization $M$: 1.9 $\mu_B$/Fe in $Fe_2B$ and 0.76 $\mu_B$/Co in $Co_2B$. In $Fe_2B$ it is only slightly overestimated, but in $Co_2B$ it is much too large at about 1.1 $\mu_B$/Co in all density-functional calculations. The relatively small spin moment of Co indicates a pronounced itinerant character of magnetism in $Co_2B$, which tends to be sensitive to quantum spin fluctuations. Therefore, we introduced a scaling factor for the local part of the effective magnetic field in the GGA functional for the Co atoms and adjusted it to match the experimental magnetization. The resulting scaling factor of 0.80 was then used for Co atoms at all concentrations. The spin moments on different atoms and the total spin magnetization obtained in this way are shown in Fig. 2. While the Fe spin moment is almost constant, the Co spin moment declines with $x$. Moreover, this decline accelerates at $x \gtrsim 0.6$, which is in excellent agreement with experimental data.[3]

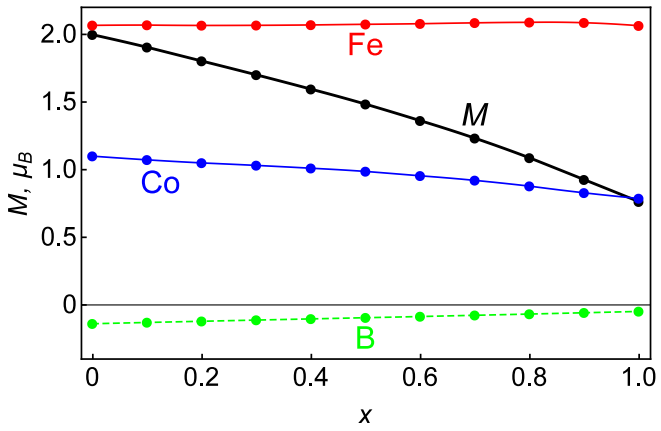


FIG. 2. Spin moments on different atoms and the total spin magnetization $M$ per transition-metal atom.

The MCA energy $K$ was obtained by calculating the single-particle energy difference for in-plane and out-of-plane orientations of the magnetization while keeping the LMTO charges fixed at their self-consistent values found without SO coupling. A uniform mesh of $30^3$ points in the full Brillouin zone provided sufficient accuracy for the $\mathbf{k}$ integration. We have verified that the values of $K$ for pure $Fe_2B$ and $Co_2B$ agree very well with Hamiltonian LMTO results. The concentration dependence of $K$ is shown in Fig. 1. The agreement with low-temperature experimental data is remarkably good, suggesting that the electronic mechanisms of MCA are correctly captured in the calculations. If the spin moment of Co is not corrected by scaling the exchange-correlation field, the downward trend in $K$ at the Co-rich end continues to large negative values in disagreement with experiment.

In $3d$ systems the SO band shifts are usually well described by second-order perturbation theory, except perhaps in small regions of the Brillouin zone. Consequently, when MCA appears in second order in SO coupling (as in the tetragonal system under consideration), the anisotropy of the expectation value of the SO operator $\Delta E_{SO} = \langle V_{SO}\rangle_x - \langle V_{SO}\rangle_z$ is approximately equal to $2K$.[13] (Here $x$ or $z$ shows the orientation of the magnetization axis.) We therefore denote $K_{SO} = \Delta E_{SO}/2$ and use the expression $2\langle \mathbf{SL}\rangle = \langle L_{z'}\rangle_{\uparrow\uparrow} - \langle L_{z'}\rangle_{\downarrow\downarrow} + \langle L_+\rangle_{\downarrow\uparrow} + \langle L_-\rangle_{\uparrow\downarrow}$ to separate the contributions to $K$ by pairs of spin channels. Here we use $L_{z'}$ to denote the component of $\mathbf{L}$ parallel to the magnetization axis, to avoid confusion with the crystallographic $z$ axis; $L_\pm$ are the usual linear combinations of the other two (primed) components of $\mathbf{L}$. The contributions $K_{\sigma\sigma'}$ to $K_{SO}$ are accumulated as energy integrals taking into account the energy dependence of the SO coupling parameters. The results for $K_{SO}$ and $K_{\sigma\sigma'}$ are shown in Fig. 1. First, we see that $K_{SO}$ is close to $K$, confirming the validity of this analysis. Second, the nonmonotonic concentration dependence of $K$ is almost entirely due to $K_{\downarrow\downarrow}$ for $x \lesssim 0.7$. While $K_{\uparrow\uparrow}$ is sizeable, it depends weakly on $x$ in this region. Additional discussion about the spin decomposition of MCA is provided in the supplementary material.[13]

Let us now analyze the electronic structure and the details of SO coupling-induced mixing for the minority-spin electrons. To resolve the minority-spin contribution to $K$ by wave vector $\mathbf{k}$, we calculated the minority-spin spectral function in the presence of SO coupling and found its first energy moment at each $\mathbf{k}$. Fig. 3 shows the difference of these integrals for magnetization along the $x$ and $z$ axes at three key concentrations: pure $Fe_2B$ ($x = 0$), the maximum of $K$ ($x = 0.3$) and its minimum ($x = 0.8$). We have checked that the Brillouin zone integral of the $\mathbf{k}$-resolved MCA energy (summed up over both spins) agrees almost exactly with the value of $K$ calculated in the usual way.

Fig. 3 shows that the MCA energy accumulates over a fairly large part of the Brillouin zone. At $x = 0$ negative contributions to $K$ dominate over most of the Brillouin zone. At $x = 0.3$ both positive and negative contributions are small. At $x = 0.8$ there are regions with large positive and large negative contributions. Overall, it appears that the most important contributions come from the vicinity of the ΓXM ($k_z = 0$) plane and from the vicinity of the ΓH ($k_x = k_y = 0$) line.

The partial minority-spin spectral functions for the transition-metal site are displayed in Fig. 4 (panels (a)-(c)) along the important high-symmetry directions for the same three concentrations. The coloring in this figure resolves the contributions from different $3d$ orbitals. At $x = 0$ the spectral function resolves the conventional electronic bands of pure $Fe_2B$ (an imaginary part of 0.004

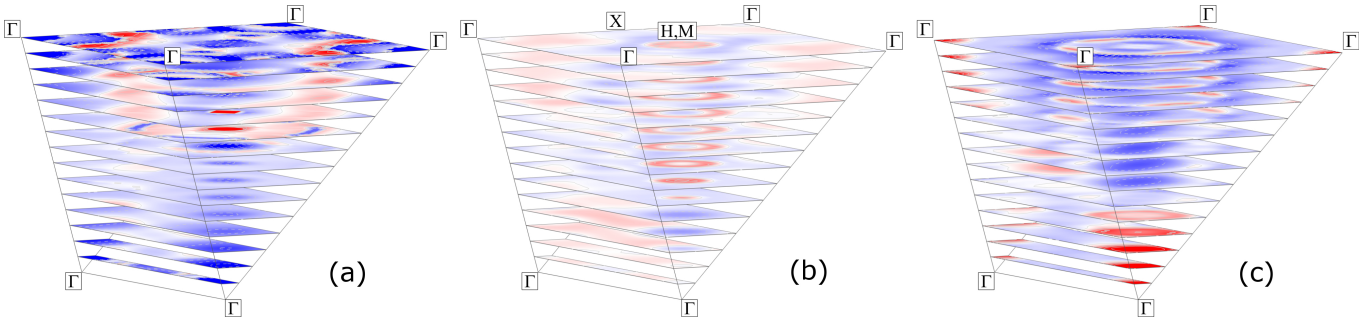


FIG. 3. Brillouin zone map of the **k**-resolved minority-spin contribution to $K$ at: (a) $x = 0$, (b) $x = 0.3$, (c) $x = 0.8$. Half of the Brillouin zone is shown; the top face of the plot is $k_z = 0$. Points H (same as M) and X are shown in panel (b). The color intensity indicates the magnitude of negative (blue) and positive (red) values.

eV is added to the energy to acquire them). At $x = 0.3$ and $x = 0.8$ substitutional disorder broadens the bands by a few tenths of an electronvolt, but their identity is in most cases preserved. Thus, we will discuss the SO-induced band mixing in the alloy, bearing in mind that band broadening should reduce the values of MCA at intermediate $x$.

As we have learned above, the dominant concentration dependence of $K$ comes from the $\langle L_{z'}\rangle_{\downarrow\downarrow}$ term, where $z'$ is the magnetization axis. The electronic states on the whole ΓXM plane can be classified as even or odd under reflection $z \to -z$. Even (odd) states have $m = 0, \pm 2$ ($m = \pm 1$) character and appear red and green (blue) in Fig. 4. States of different parity do not intermix on this plane in the absence of SO coupling, as is clearly seen in Fig. 4a. The selection rules for SO coupling of the minority-spin states follow from the definite parity of the components of $\hat{\mathbf{L}}$ under reflection. $\hat{L}_z$ (even; relevant for $\mathbf{M} \parallel z$) only mixes states of the same parity on the ΓXM plane, or more generally orbitals of the same $m$. Coupling between states of the $m = \pm 2$ character (red) is stronger compared to states of the $m = \pm 1$ character (blue). In contrast, $\hat{L}_x$ (odd; relevant for $\mathbf{M} \parallel x$) couples states of the opposite parity on the ΓXM plane, or more generally orbitals $m$ and $m \pm 1$. All these couplings contribute to $K$ only when the Fermi level lies between the two states that are being coupled. Whenever $\hat{L}_z$ or $\hat{L}_x$ couples such states, there is a negative contribution to the energy of the system with the corresponding direction of $\mathbf{M}$.

With the help of Fig. 4 we can now deduce which couplings contribute to $K$ at different concentrations. At $x = 0$ the Fermi level lies between the filled even states (bands 1-2) and empty odd states (bands 3-4) near Γ. Coupling of these states by $\hat{L}_x$ contributes to negative $K$. Filling of the hole pocket at Γ (bands 3-4) with increasing $x$ suppresses this contribution. At $x = 0.3$ the odd bands 3-4 are filled (Fig. 4b), and the minority-spin contribution to $K$ is small (Fig. 3b). These two cases are sketched in Fig. 4d.

At still larger $x$ the odd band 5 gets gradually filled, activating the negative contribution to $K$ from the mixing of band 5 with empty even bands 6-7. This trend continues till about $x = 0.8$, where an even pair of bands 6-7 (degenerate at Γ) begins to fill (Fig. 4c). Mixing of these bands by $\hat{L}_z$ leads to an intense positive contribution to $K$ near the Γ point (clearly seen in Fig. 3c), and the trend reverses again. Thus, the nonmonotonic dependence of $K$ in the whole concentration range is explained. Note that if the exchange-correlation field on the Co atoms is not scaled down to bring the magnetization in agreement with experiment, the exchange splitting remains too large, and bands 6-7 remain empty up to $x = 1$. As a result, without this correction the uninterrupted negative trend brings $K$ to large negative values in disagreement with experiment.

To assess the effect of atomic relaxations on $K$, we optimized all inequivalent structures with two formula units per unit cell using the VASP code[15] and the GGA. The volumes were fixed at the same values as in the CPA studies at the same $x$, while the cell shape and internal coordinates were relaxed. Since all these supercells preserve the $\sigma_z$ reflection plane, the displacements of Fe and Co atoms are confined to the $xy$ plane. All displacements were less than 0.025 Å. One of the two structures at $x = 0.5$ breaks the $C_4$ symmetry. For this structure we took the average of the energies for $\mathbf{M} \parallel x$ and $\mathbf{M} \parallel y$ as the in-plane value in the calculation of $K$, which corresponds to the averaging over different orientations of the same local ordering.

The changes in the absolute value of $K$ due to the relaxation and its values (meV/f.u.) in the relaxed structures were found to be: $-26\%$ and $-0.11$ in $Fe_2B$, $-6\%$ and 0.25 in $Fe_{1.5}Co_{0.5}B$, $-13\%$ and 0.15 in the FeCoB [100] superlattice, 6% and 0.12 in the FeCoB [110] superlattice, $-11\%$ and $-0.31$ in $Fe_{0.5}Co_{1.5}B$), and $-19\%$ and $-0.04$ in $Co_2B$. While MCA tends to be larger for ordered structures, the concentration trend in supercell calculations agrees well with the CPA results for disordered alloys. Although this set of unit cells is limited, the results suggest that local relaxations do not qualitatively change the concentration dependence shown in Fig. 1.

Larger positive values of $K$ are favorable for permanent magnet applications. Our electronic structure analysis shows that the maximum near $x \approx 0.3$ corresponds

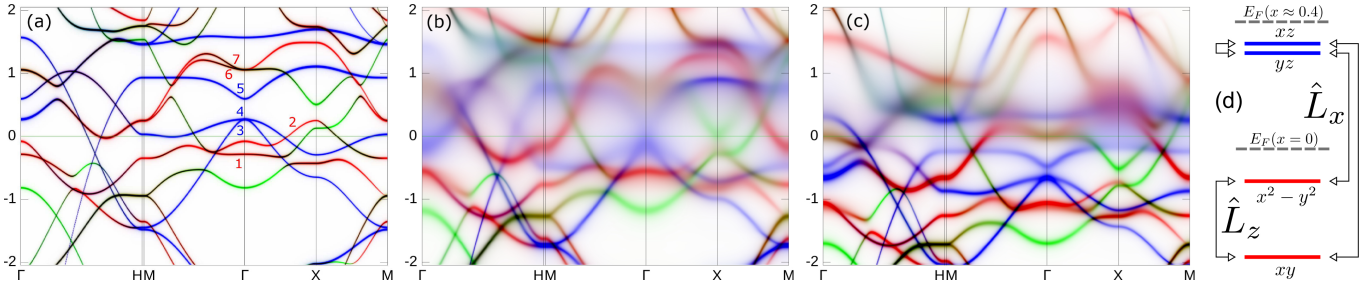


FIG. 4. (a-c) Minority-spin partial spectral functions for the transition-metal site in the absence of SO coupling at (a) $x = 0$, (b) $x = 0.3$, and (c) $x = 0.8$. Energy is in eV. (d) Level diagram and SO selection rules at the Γ point (bands 1-4). Color encodes the orbital character of the states. The intensities of the red, blue and green color channels are proportional to the sum of $xy$ and $x^2 - y^2$ ($m = \pm 2$), sum of $xz$ and $yz$ ($m = \pm 1$), and $z^2$ ($m = 0$) character, respectively.

to the optimal band filling. Further raising of $K$ requires favorable changes in the band structure, which could be induced by epitaxial or chemical strain. We therefore considered the dependence of $K$ at $x = 0.3$ on the volume-conserving tetragonal distortion. The results plotted in Fig. 5 show a very strong effect: $K$ is doubled under a modest 3% increase in $c/a$ due to the sharply increasing spin-flip contributions. A more detailed analysis shows that the latter is largely due to the increase in the $c$ parameter. On the other hand, the minority-spin contribution increases with decreasing volume. Thus, increasing $c$ and decreasing $a$ both have a positive effect on MCA. This enhancement could be achieved through epitaxial multilayer engineering. The search for a suitable alloying element to enhance the $c/a$ ratio is an interesting subject for further investigation.

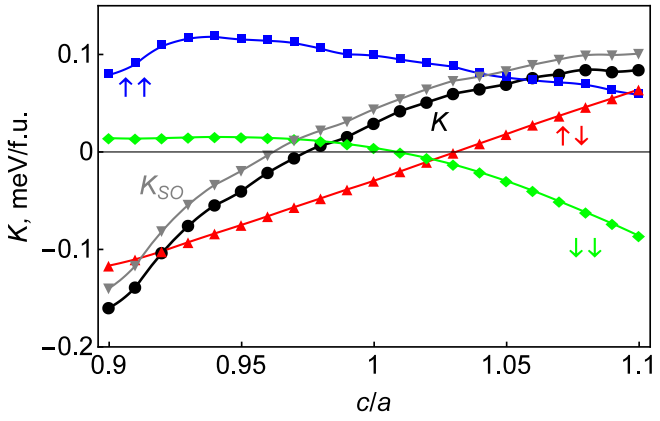


FIG. 5. MCA energy $K$ as a function of the $c/a$ ratio at $x = 0.3$ (the value $c/a = 1$ is assigned to the unstrained lattice). $K_{SO}$ and $K_{\sigma\sigma'}$ are also shown.

In conclusion, we have explained how the spin reorientation transitions in $(Fe_{1-x}Co_x)_2B$ alloys originate in the SO selection rules and the consecutive filling of minority-spin electronic bands of particular orbital character. Near the optimal 30% concentration of Co, the MCA energy is predicted to increase quickly with the $c/a$ ratio, which could be implemented by epitaxial strain or a suitable chemical doping.

The work at UNL was supported by the National Science Foundation through Grant No. DMR-1308751 and performed utilizing the Holland Computing Center of the University of Nebraska. Work at Ames Lab and LLNL was supported in part by the Critical Materials Institute, an Energy Innovation Hub funded by the US DOE and by the Office of Basic Energy Science, Division of Materials Science and Engineering. Ames Laboratory is operated for the US DOE by Iowa State University under Contract No. DE-AC02-07CH11358. Lawrence Livermore National Laboratory is operated for the US DOE under Contract DE-AC52-07NA27344.

[1] J. Stohr and H. Siegmann, in *Magnetism: From fundamentals to Nanoscale Dynamics* (Springer, Berlin, 2006), p. 805.
[2] A. Iga, Jpn. J. Appl. Phys. **9**, 415 (1970).
[3] M. C. Cadeville and I. Vincze, J. Phys.: Metal Phys. **5**, 790 (1975).
[4] L. Takacs, M. C. Cadeville, and I. Vincze, J. Phys. F: Metal Phys. **5**, 800 (1975).
[5] W. Coene, F. Hakkens, R. Coehoorn, D. B. de Mooij, C. de Waard, J. Fidler and R. Grössinger, J. Magn. Magn. Mater. **96**, 189 (1991).
[6] M. D. Kuz'min, K. P. Skokov, H. Jian, I. Radulov and O. Gutfleisch, J. Phys.: Condens. Matter **26**, 064205 (2014).
[7] C. Kapfenberger, B. Albert, R. Pöttgen, and H. Huppertz, Z. Kristallogr. **221**, 477 (2006).
[8] L. H. Lewis and F. Jiménez-Villacorta, Metall. Mater. Trans. A **44**, 2 (2013).
[9] P. C. Canfield and Z. Fisk, Philos. Mag. B **65**, 1117 (1992).
[10] A. Aharoni, J. Appl. Phys. **83**, 3432 (1998).
[11] I. Turek, V. Drchal, J. Kudrnovský, M. Šob, and P. Weinberger, *Electronic structure of disordered alloys, surfaces and interfaces* (Kluwer, Boston, 1997).
[12] L. Ke, K. D. Belashchenko, M. van Schilfgaarde, T. Kotani, and V. P. Antropov, Phys. Rev. B **88**, 024404 (2013).
[13] See supplementary material at [...] for implementation details, explanation about $K_{SO}$, and the discussion of orbital moment anisotropy.
[14] J. P. Perdew, K. Burke, and M. Ernzerhof, Phys. Rev. Lett. **77**, 3865 (1996); **78**, 1396 (1997).
[15] G. Kresse and J. Furthmüller, Comput. Mat. Sci. **6**, 15 (1996).

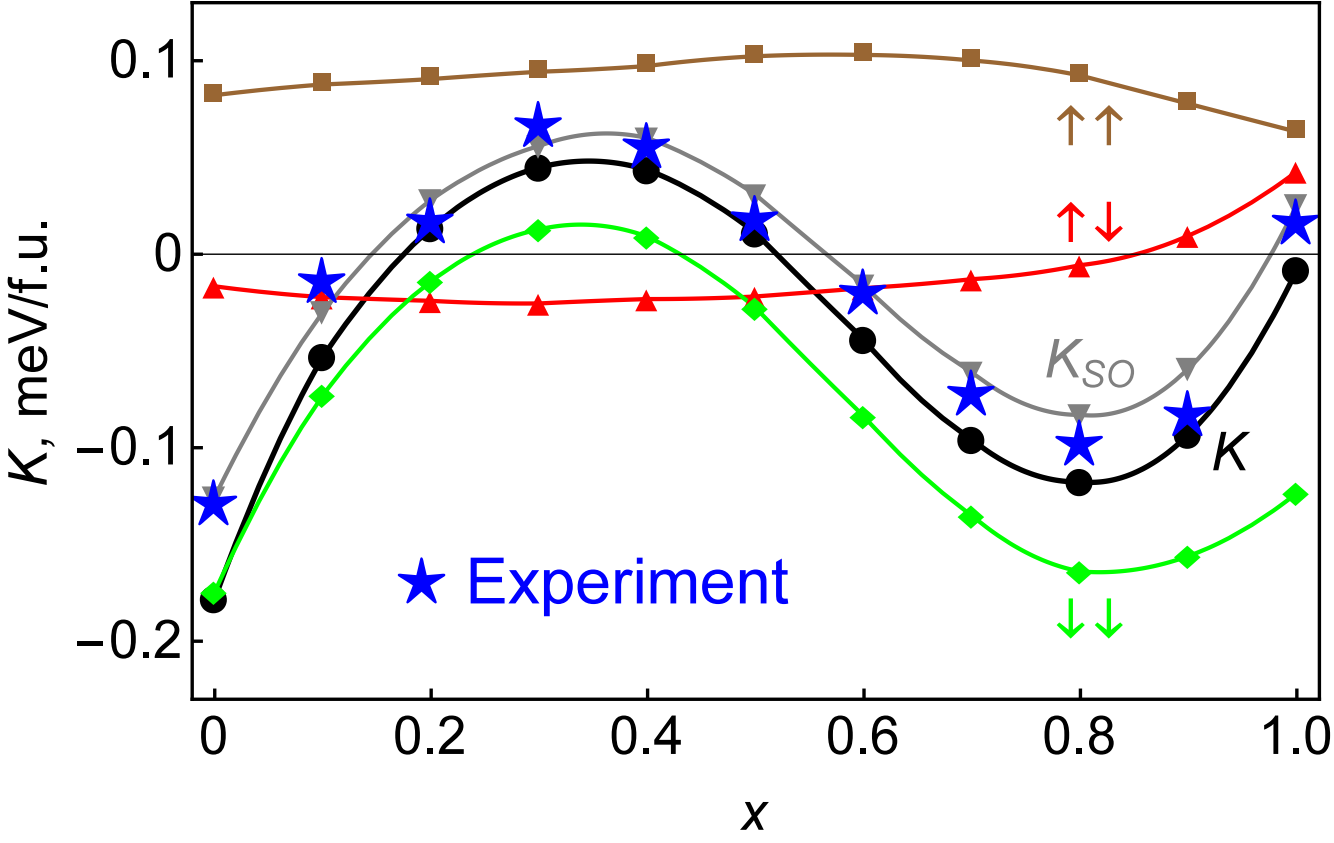
0.1
0
−0.1
−0.2
K, meV/f.u.
0
0.2
0.4
0.6
0.8
1.0
x
↑↑
↑↓
↓↓
K_SO
K
★ Experiment

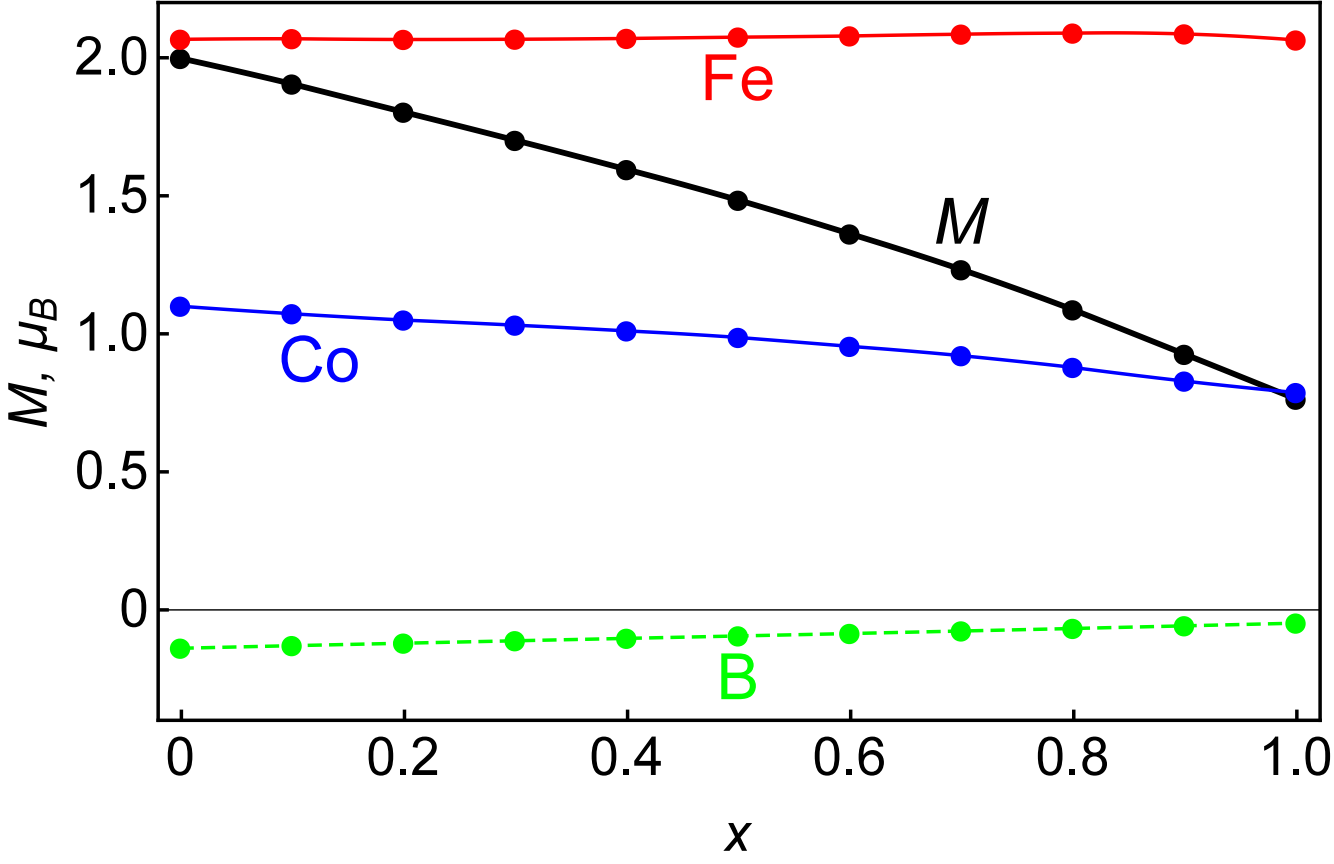
Fe
M
Co
B
M, μB
x
2.0
1.5
1.0
0.5
0
0
0.2
0.4
0.6
0.8
1.0

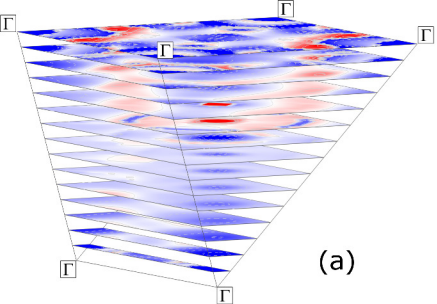
Γ
Γ
Γ
Γ
Γ
(a)
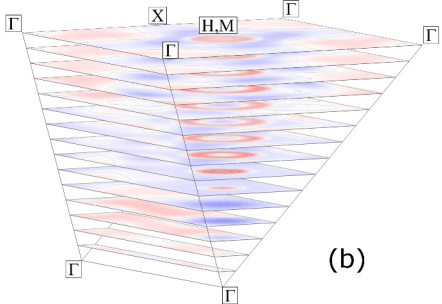
Γ
X
H,M
Γ
Γ
Γ
Γ
(b)
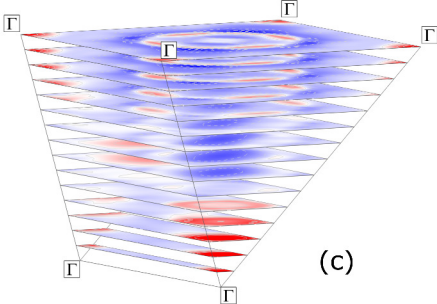
Γ
Γ
Γ
Γ
Γ
(c)

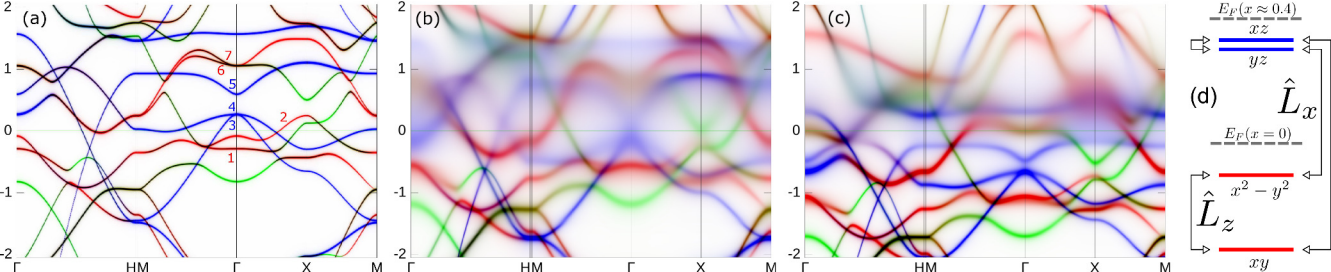
(a)
(b)
(c)
(d)
2
1
0
-1
-2
Γ
HM
Γ
X
M
7
6
5
4
3
2
1
$E_F(x \approx 0.4)$
$xz$
$yz$
$\hat{L}_x$
$E_F(x = 0)$
$x^2 - y^2$
$\hat{L}_z$
$xy$

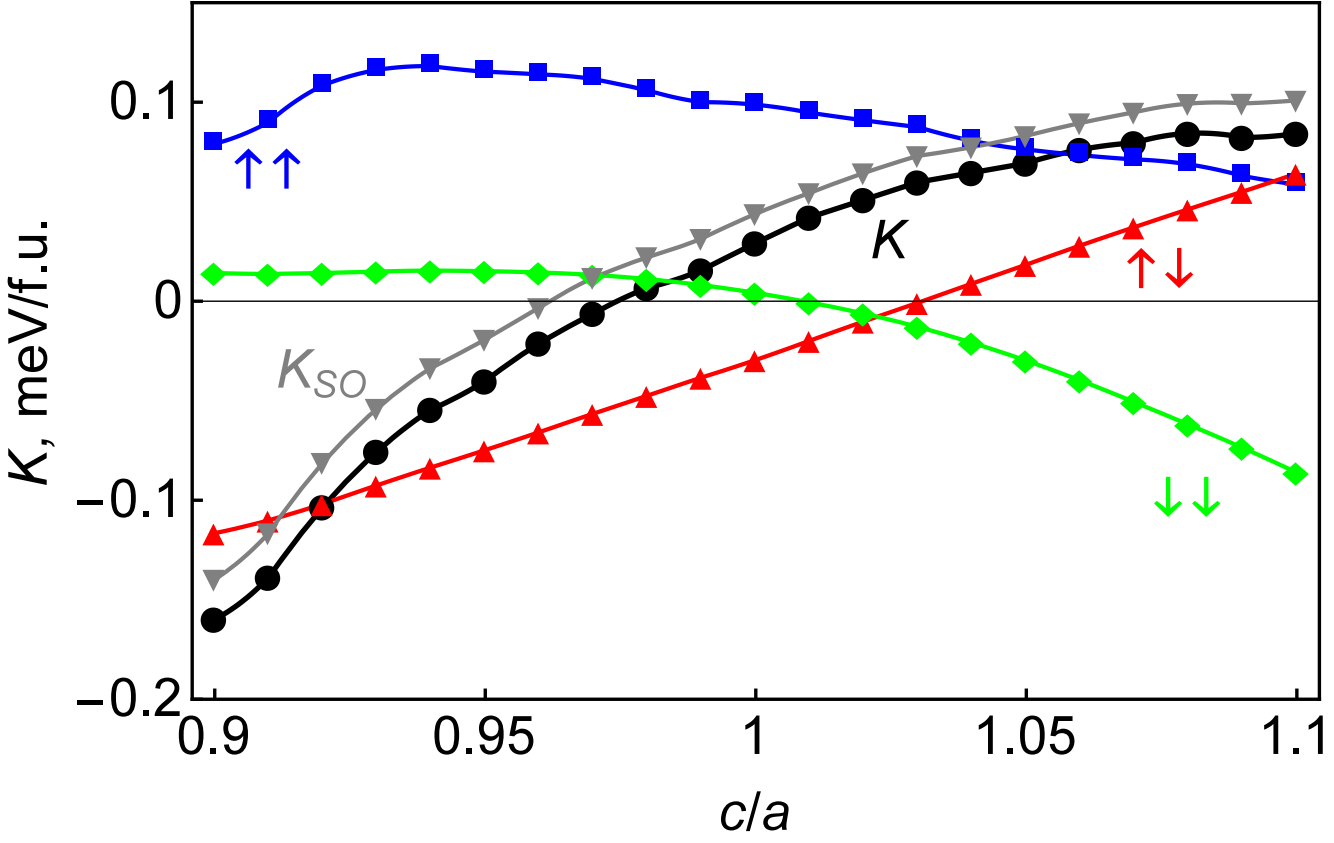
0.1
0
−0.1
−0.2
0.9
0.95
1
1.05
1.1
K, meV/f.u.
c/a
↑↑
↓↓
↑↓
K
K_SO